ONCOIMMUNOLOGY
2016, VOL. 5, NO. 8, e1191731 (15 pages)
http://dx.doi.org/10.1080/2162402X.2016.1191731

Taylor & Francis
Taylor & Francis Group

ORIGINAL RESEARCH

Warburg metabolism in tumor-conditioned macrophages promotes metastasis in human pancreatic ductal adenocarcinoma

Hweixian Leong Penny[a], Je Lin Sieow[a], Giulia Adriani[b], Wei Hseun Yeap[a], Peter See Chi Ee[a], Boris San Luis[a], Bernett Lee[a], Terence Lee[c], Shi Ya Mak[d], Ying Swan Ho[d], Kong Peng Lam[d], Choon Kiat Ong[e], Ruby Y. J. Huang[f], Florent Ginhoux[a], Olaf Rotzschke[a], Roger D. Kamm[b,g], and Siew Cheng Wong[a]

[a]Singapore Immunology Network (SIgN), Biomedical Sciences Institute, A*STAR, Immunos, Singapore; [b]BioSystems and Micromechanics IRG, Singapore-MIT Alliance for Research and Technology (SMART), Singapore; [c]Raffles Institution, Singapore; [d]Bioprocessing Technology Institute, A*STAR, Centros, Singapore; [e]NCCS-VARI Translational Research Laboratory, National Cancer Center, Singapore; [f]Centre for Translational Medicine NUS Yong Loo Lin School of Medicine, CSI Singapore, Singapore; [g]Department of Biological Engineering, Massachusetts Institute of Technology, Cambridge, MA, USA

ABSTRACT

Patients with pancreatic ductal adenocarcinoma (PDAC) face a clinically intractable disease with poor survival rates, attributed to exceptionally high levels of metastasis. Epithelial-to-mesenchymal transition (EMT) is pronounced at inflammatory foci within the tumor; however, the immunological mechanisms promoting tumor dissemination remain unclear. It is well established that tumors exhibit the Warburg effect, a preferential use of glycolysis for energy production, even in the presence of oxygen, to support rapid growth. We hypothesized that the metabolic pathways utilized by tumor-infiltrating macrophages are altered in PDAC, conferring a pro-metastatic phenotype. We generated tumor-conditioned macrophages *in vitro*, in which human peripheral blood monocytes were cultured with conditioned media generated from normal pancreatic or PDAC cell lines to obtain steady-state and tumor-associated macrophages (TAMs), respectively. Compared with steady-state macrophages, TAMs promoted vascular network formation, augmented extravasation of tumor cells out of blood vessels, and induced higher levels of EMT. TAMs exhibited a pronounced glycolytic signature in a metabolic flux assay, corresponding with elevated glycolytic gene transcript levels. Inhibiting glycolysis in TAMs with a competitive inhibitor to Hexokinase II (HK2), 2-deoxyglucose (2DG), was sufficient to disrupt this pro-metastatic phenotype, reversing the observed increases in TAM-supported angiogenesis, extravasation, and EMT. Our results indicate a key role for metabolic reprogramming of tumor-infiltrating macrophages in PDAC metastasis, and highlight the therapeutic potential of using pharmacologics to modulate these metabolic pathways.

ARTICLE HISTORY
Received 11 January 2016
Revised 12 May 2016
Accepted 15 May 2016

KEYWORDS
Metabolism; macrophages; metastasis; pancreatic cancer

Introduction

Pancreatic ductal adenocarcinoma (PDAC) is a leading cause of cancer mortality globally. With an overall 5-year survival rate of 3–5%, incidence almost equals mortality.[1] However, the mechanisms underlying the highly metastatic nature of this malignancy remain poorly understood. Studies in mouse models of PDAC demonstrated that epithelial-to-mesenchymal transition (EMT), a hallmark of metastasis, is most pervasive at inflammatory foci within the tumor.[2] Induction of pancreatitis increased the number of circulating pancreatic tumor cells, while immunosuppression using dexamethasone therapy abrogated dissemination.[2] In addition, cells already having undergone EMT have been identified in precursor lesions, known as Pancreatic Intraepithelial Neoplasia (PanINs), suggesting that initiation of metastasis occurs prior to the development of frank carcinoma.[2] Taken together, these results support the notion that inflammation can facilitate tumor dissemination, and may represent one of the early events of cellular invasion in PDAC. Hence, studying the immune cell infiltrate in PDAC may shed light on its particularly metastatic nature.

Highly predominant in many tumors, macrophages were originally perceived to be involved in antitumor immunity. However, overwhelming clinical and experimental evidence now indicate that in many cases, tumor-associated macrophages (TAMs) enhance chronic inflammation, stimulating angiogenesis, migration, and invasion.[3] Using mouse models of mammary carcinoma, Qian and colleagues showed that a distinct population of host macrophages was recruited to extravasating pulmonary metastases.[4] Systematic ablation of this population via both genetic and chemical approaches indicated that these macrophages were necessary for efficient metastatic seeding. Building upon this, Kitamura and colleagues from the same group recently reported that in the same animal model, the macrophages that were not only recruited, but also retained at the metastatic site (lung), promoted extravasation of tumor cells.[5]

During inflammation, macrophages adopt distinct metabolic signatures as they switch from quiescent to activated states.[6] Emerging evidence suggests that these metabolic pathways themselves can direct immune cell differentiation and instruct effector function. For instance, Haschemi and colleagues have

CONTACT Siew Cheng Wong wong_siew_cheng@immunol.a-star.edu.sg Singapore Immunology Network, 8A Biomedical Grove, Immunos #04-04, Singapore.
Supplemental data for this article can be accessed on the publisher's website.

shown that modulation of a kinase involved in glucose metabolism can alter macrophage phenotype, influencing cytokine production and the expression of key surface receptors.[7] Several studies have reported the contribution of other key glycolytic enzymes such as PDK1,[8] PKM2,[9] PFKFB3[10,11] to the inflammatory state of M1, LPS-activated and atherosclerotic macrophages, respectively. Thus, we postulated that metabolic states in TAMs might play a role in directing their tumor response. Large numbers of macrophages have been reported to infiltrate the pre-neoplastic lesions of PDAC,[12] but the metabolic program utilized by these cells is unclear. How these programs, in turn, affect tumor growth, dissemination, and seeding at distal sites is completely unknown. Here, we ask how macrophage commitment to specific metabolic fates in PDAC influences their capacity to promote tumor dissemination.

Results

Generation of TAMs

To address how macrophage metabolism affects tumor outcomes, we utilized an *in vitro* model of tumor-conditioned macrophages. Conditioned media from normal (HPNE) or PDAC (Panc1 or MiaPaCa2) cell lines were incubated with peripheral blood monocytes from healthy donors to generate normal pancreatic "resident" macrophages and TAMs, respectively. These conditioned macrophages were validated as *bona fide* macrophages on the basis of morphology, endocytic capacity, and marker expression (Fig. 1A-C). All three cell types exhibited characteristic spindly- and "fried-egg"-shaped morphology (Fig. 1A), with similar endocytic capacity (Fig. 1B). Classical macrophage markers were also expressed, including CD68, CD163, M-CSFR, and CD206, although Panc1 and MiaPaCa2 macrophages expressed significantly higher levels of CD163 and CD206 compared with their HPNE counterparts (Fig. 1C). A higher proportion of Annexin-V-positive HPNE macrophages were detected, but all three macrophage types had similar viability as assessed by DAPI (Fig. 1D). Interestingly, Panc1 and MiaPaCa2 macrophages expressed higher transcript levels of the "classically-activated M1" markers, *IL-1β*, *IL-6*, *TNF-α*, and *CCL3*, and the "alternatively-activated M2" marker, *Arg1*, suggesting that these TAMs exhibit a mixed macrophage phenotype (Fig. 1E). Other M1 and M2 genes, such as *IL-4* and *iNOS*, were assayed, but expression levels were too low to be of functional significance.

Pro-metastatic capabilities of TAMs

To determine the pro-metastatic capabilities of these TAMs, we collected the supernatants from the macrophage cultures to assess their capacity to induce new blood vessel formation (angiogenesis), promote tumor cells to seed secondary sites (extravasation), and boost EMT. They will be hereafter referred to as HPNE mac-sup and TAM-sup for macrophages differentiated in HPNE- and PDAC- conditioned media, respectively.

In a classical human umbilical vein endothelial cell (HUVEC) network-formation assay, TAM-sups consistently supported 1.5–2-fold higher formation of HUVEC networks compared with their HPNE counterparts (Fig. 2). Quantitative analysis of key metrics detected significant increases in total network length, total branch points, and total loops formed, with a concomitant decrease in the number of total nets (incomplete loops) in TAM-sup supported networks (Fig. 2B-E). Therefore, we hypothesized that TAMs may accelerate angiogenesis in a VEGF-dependent manner. Consistent with this, TAMs were found to express significantly higher transcript levels of *VEGFA* (Fig. 2F). Furthermore, neutralization of VEGFA in the macrophage supernatants with an anti-VEGFA antibody demonstrated that the TAMs promote angiogenesis in a VEGF-dependent manner (Fig. 2G).

To mimic cancer cell extravasation in 3D, a microfluidic device as shown in Fig. 3 consisting of a central gel channel flanked by two fluidic channels was utilized. Similar microfluidic platforms have been used for investigating angiogenesis,[13,14] EMT,[15,16] cancer cell–macrophage interactions,[17] intravasation[18] and extravasation.[19,20] For the present work, GFP-expressing HUVECs were seeded into one of the fluidic channels to form a uniform monolayer mimicking a blood vessel wall (Fig. 3A). Labeled PDAC tumor cells, with or without their corresponding conditioned macrophages, were then seeded into the "blood vessel" and the number of tumor cells that extravasated through the blood vessel wall into the matrix was measured by confocal microscopy (Fig. 3B). Remarkably, both Panc1 and MiaPaCa2 macrophages promoted the extravasation of Panc1 and MiaPaCa2 tumor cells, respectively, by 3–4-fold compared with control HPNE macrophages, indicating that these TAMs promote mobilization of tumor cells (Fig. 3C). As VEGF has also been shown to increase vascular permeability to permit extravasation of tumor cells,[21] the elevated production of *VEGFA* in the TAMs (as shown in Fig. 2F) is a likely explanation for the promotion of both extravasation and angiogenesis.

During development, EMT is a naturally occurring process by which epithelial cells undergo profound changes in gene expression and cell morphology in preparation for increased cell mobility through tissues.[22] During the process of EMT, epithelial markers, including tight junction and adherens junction proteins, such as E-cadherin, desmoplakin, and ErbB3, are lost as the cells begin to move apart. Mesenchymal markers, such as Snail, Vimentin, and Zeb1/2 are upregulated, and columnar or cuboidal cells adopt a flattened, spindly morphology in preparation for crossing the tissue layers.

During the initiation of metastasis, it is thought that tumor cells at the leading edge of the tumor undergo a similar process of EMT, facilitating migration to secondary organs.[21] Consistent with the detected increases in angiogenesis and extravasation, Panc1 and MiaPaCa2 mac-sups induced greater spreading of pancreatic epithelial HPAF-II colonies compared with their HPNE counterparts (Fig. 4A). This result is quantitatively illustrated by the significantly increased internuclear distance between two neighboring cells in the HPAF-II colonies incubated with TAM-sups (Fig. 4B). In addition, compared with HPNE mac-sup, TAM-sups promoted a greater loss of the adherens junction protein E-cadherin (Fig. 4A, C). Staining of HPAF-II cells with phalloidin, which binds polymerizing F-actin, detected an increase in the cell area of HPAF-II colonies incubated with TAM-sups compared to HPNE mac-sup, although this did not reach statistical significance (Fig. 4D).

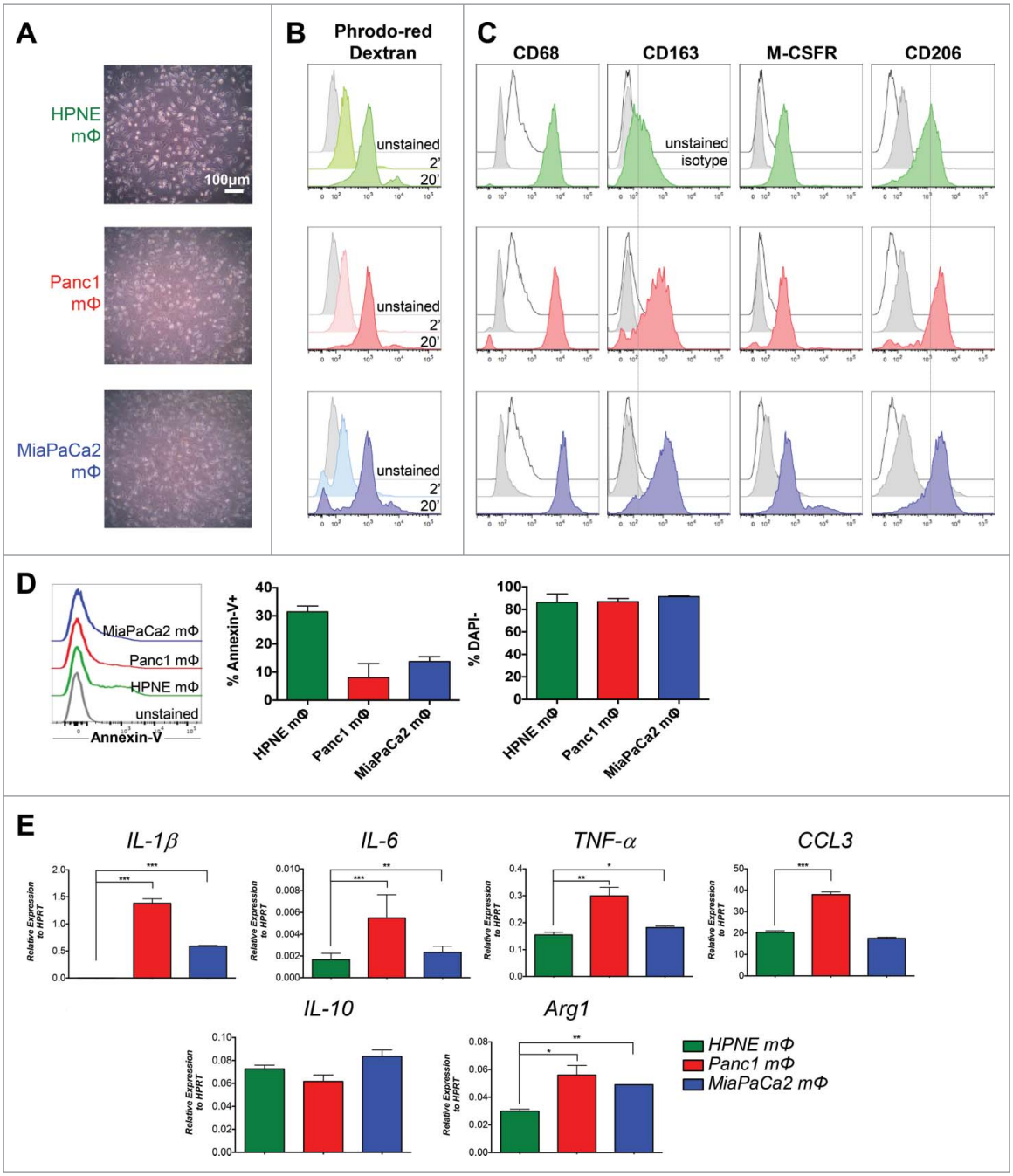

Figure 1. Validation of *in-vitro*-generated mΦ. (A) $CD14^+$ MACS-isolated peripheral blood monocytes from healthy donors were cultured with HPNE-, Panc1- and MiaPaCa2-conditioned media for 7–9 d. The representative bright-field images of mΦ generated from the respective conditioned media are shown. (B) The three mΦ types were assayed for their ability to endocytose using pHrodo-Red Dextran beads. The histograms indicating uptake of the pH-sensitive red fluorescence after 2 and 20 min incubation with the beads are shown. (C) The histograms of the expression of classical mΦ markers CD68, CD163, M-CSFR and CD206 on the three mΦ types by flow cytometry are shown. Dotted lines through CD163 and CD206 histograms have been drawn to demarcate peak of HPNE mΦ stain. (A–C) First (green), second (red) and third (blue) rows denote data for HPNE, Panc1 and MiaPaCa2 mΦ, respectively. Data are representative of n = 4 independent experiments. (D) The histograms of Annexin-V staining by flow cytometry on the mΦ types are shown. Bar graphs depict the mean ± SEM of the proportion of Annexin-V^+ apoptotic cells and $DAPI^-$ live cells of total cells for the three mΦ types. Data are collated from n = 2 independent experiments. (E) MΦ are assayed for transcript expression of M1 and M2 markers *IL-1β*, *IL-6*, *TNF-α*, *IL-10* and *Arg1* by qPCR. Bar graphs shown are the mean ± SEM of the relative expression of that gene over HPRT. Data are representative of n = 3 independent experiments. $^*p < 0.05$; $^{**}p < 0.01$; $^{***}p < 0.001$.

Several classic mesenchymal markers, including N-cadherin, Zeb1/2, Snail, Slug, and Vimentin, were assayed by qPCR, but little or no upregulation in expression could be detected in these HPAF-II colonies (data not shown).

We therefore hypothesized that Panc1 and MiaPaCa2 macrophages may induce EMT via production of growth factors known to promote EMT, such as TGF*β*, HGF, EGF, and/or FGF. Indeed, compared to HPNE macrophages, we observed a 1.5–3-fold increase in *TGFβ* gene expression, and a 1.5–2-fold increase in *HGF* gene expression in MiaPaCa2 and Panc1 macrophages, respectively. Expression of *EGF* and *FGF* was negligible in all three macrophage types.

To determine whether TAMs induced EMT via an HGF and/or TGF*β*-dependent manner, neutralizing antibodies

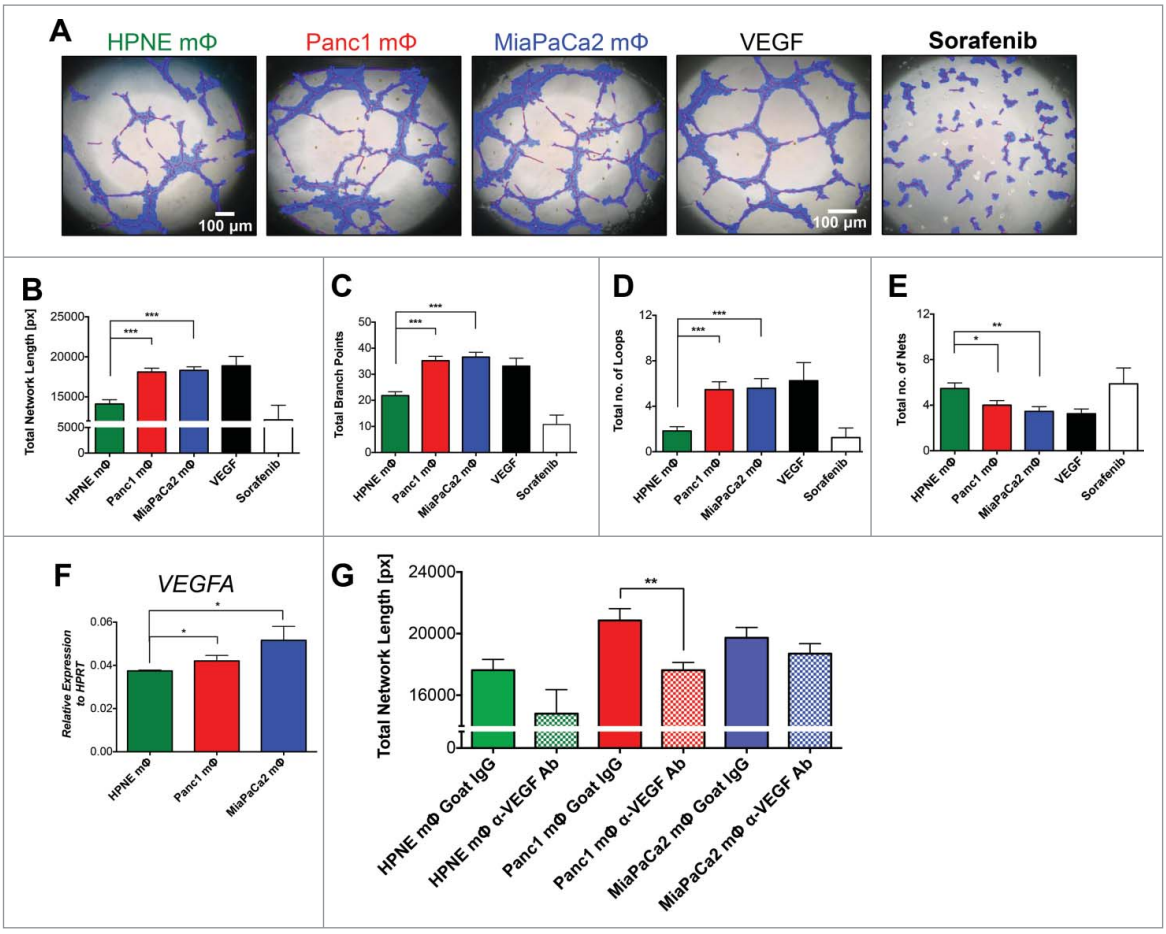

Figure 2. Panc1 and MiaPaCa2 mΦ promote higher rates of angiogenesis compared to HPNE mΦ. MΦ supernatants (sups) harvested from the three mΦ types were added to 1×10^4 HUVECs grown on top of matrigel per well of Ibidi's μ-angiogenesis slide for 4 h at 37°C. 200 ng/mL rhVEGF-A and 10 μM of VEGFR inhibitor Sorafenib were used as a positive and negative control, respectively. (A) The representative bright-field images of HUVEC networks analyzed by Ibidi's WimTube Image Analysis software are shown. (B) Total network length (networks identified by red lines, length of tubes identified by blue regions), (C) total branch points, (D) total loops (identified by small yellow numbers) and (E) total nets are depicted in bar graphs as mean ± SEM of collated data from n = 6 independent experiments. (F) A bar graph of mean ± SEM of the expression of VEGFA by qPCR in the respective mΦ is shown. Data are representative of n = 3 independent experiments. (G) Shown are bar graphs of total network length in which VEGFA is neutralized in the macrophage supernatants by the addition of an anti-VEGF antibody. Data is collated from n = 4 independent experiments. $^{*}p < 0.05$; $^{**}p < 0.01$; $^{***}p < 0.001$.

against HGF and/or TGFβ were added in the macrophage supernatants when performing the EMT assay. While neutralizing HGF did not result in a significant change in HPAF-II colony spreading (as shown by internuclear distance) compared to isotype control antibody, neutralizing TGFβ resulted in a pronounced reduction in colony spreading (Fig. 4F). Neutralizing both HGF and TGFβ at the same time did not have a synergistic effect in reducing colony spreading further, compared to neutralizing TGFβ alone (Fig. 4F). This suggests that TGFβ and not HGF is the key factor in promoting EMT by TAMs.

Taken together, our observations from these key parameters of metastasis strongly indicate that infiltrating PDAC TAMs have the propensity to promote a more aggressive, pro-metastatic phenotype in tumor cells.

Glycolytic profile of TAMs

To ascertain whether the pro-metastatic phenotype of TAMs was associated with a specific metabolic pathway required for such energetic needs, we utilized a live metabolic flux assay to determine their glycolytic and mitochondrial respiration (oxidative phosphorylation, OXPHOS) capacities. Notably, compared with control HPNE macrophages, Panc1 and MiaPaCa2 macrophages preferentially utilized glycolysis over OXPHOS, as observed by a 2-fold increase in glycolytic capacity (Fig. 5A) and a concomitant 2-fold decrease of mitochondrial respiration capacity (Fig. 5B). Consistent with this result, transcript analysis of key glycolytic genes revealed upregulation of *HK2, GPI, ALDOA, TPI1* and *PGK1* in TAMs compared with HPNE macrophages (Fig. 5C). In addition, L-lactate measured in macrophage lysates revealed 1.4–1.6-fold higher production of this metabolite in TAMs compared to HPNE macrophages (Fig. 5D). ROS production was also assessed, but all three macrophage types appeared to produce little ROS, with no comparable differences at the basal state (Fig. 5E). Taken together, our results show that TAMs preferentially utilize glycolysis to fulfill their energetic needs, which correlates with their pro-metastatic phenotype.

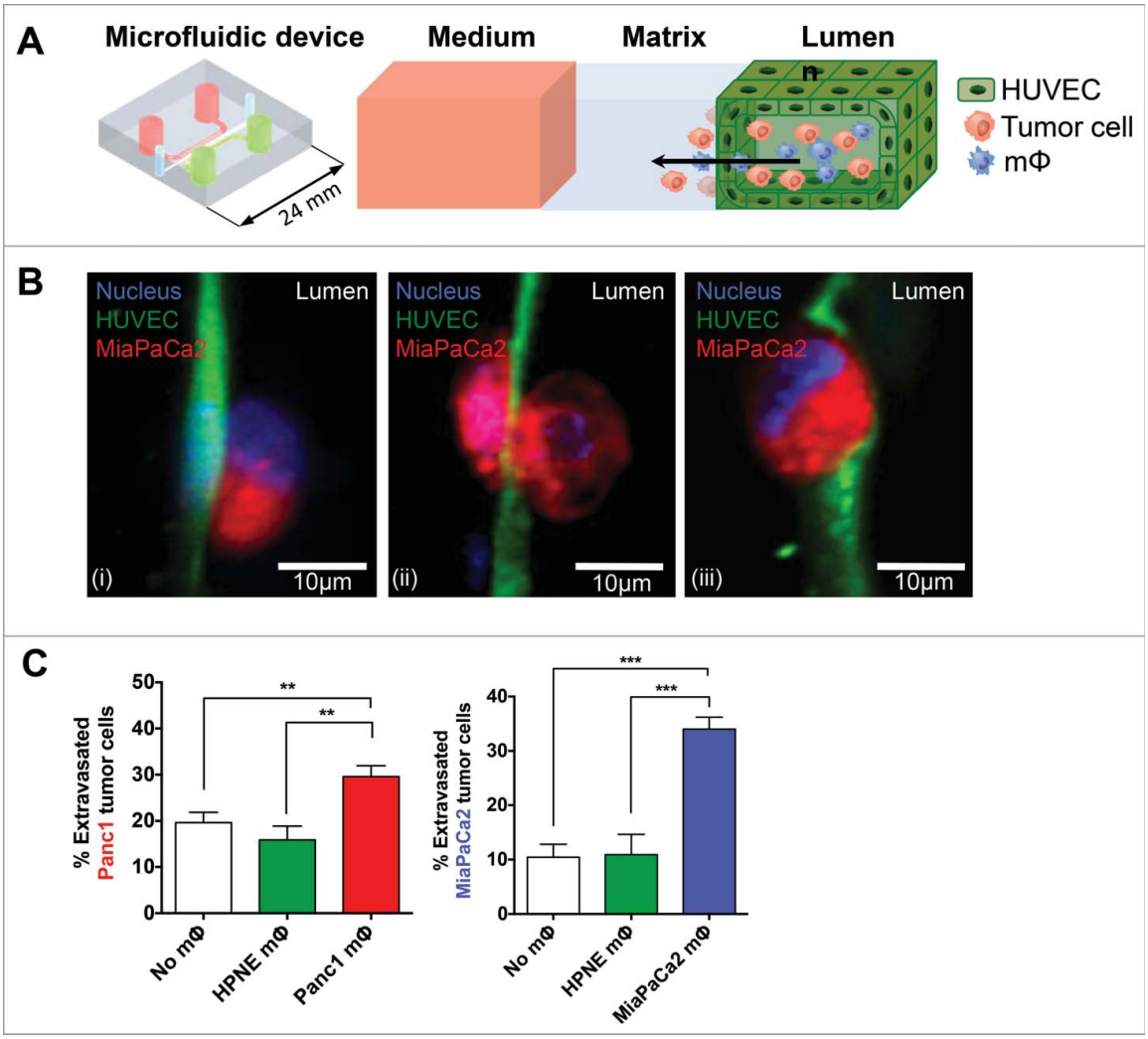

Figure 3. Panc1 and MiaPaCa2 mΦ augmented extravasation compared to HPNE mΦ. A PDMS microfluidic device consisting of a central gel region flanked by two side fluidic channels was utilized. HUVECs were cultured in a uniform monolayer mimicking a blood vessel wall in one of the fluidic channels. Panc1 or MiaPaCa2 tumor cells with or without corresponding mΦ (1:1) were co-injected into the channel containing HUVECs. After 24 h, tumor cell extravasation across the endothelial monolayer into the gel region was quantified by confocal microscopy and expressed as a percentage of the total number of cells present on the monolayer. (A) 3D drawing of the microfluidic device and an illustration of the expected movement of tumor cells and/or mΦ across the HUVEC monolayer into the 3D matrix are shown. This mimics the extravasation of cells from blood vessels into potential secondary metastatic sites. (B) The representative immunofluorescence images of MiaPaCa2 tumor cells in three different conditions after 24 h are shown: (i) not extravasated, (ii) in the process of extravasating and (iii) extravasated across the HUVEC monolayer. (C) Shown are bar graphs of mean ± SEM of the percentage of extravasated cancer cells, using collated data from at least six devices per condition. $^{**}p < 0.01; ^{***}p < 0.001$.

Effect of inhibition of glycolysis on pro-metastatic capabilities of TAMs

To address whether this pro-metastatic phenotype in TAMs is dependent on their preferential utilization of glycolysis, we inhibited glycolysis in the macrophages by targeting HK2. The enzyme HK2 catalyzes the first rate-limiting step of glycolysis, in which glucose is converted to glucose-6-phosphate, to commit each molecule of glucose to enter glycolysis in an irreversible reaction. We treated the macrophages with a competitive inhibitor of HK2, 2-deoxyglucose (2DG), and repeated the series of angiogenesis, extravasation, and EMT assays.

We first confirmed that 2DG treatment did not adversely affect cell viability. Bright-field images of the macrophages cultured for 6 h without or with 25 mM 2DG clearly show that the macrophages are alive after 2DG treatment (Fig. S1A). Inhibition of glycolysis by 2DG treatment was also verified in all three macrophage types by live metabolic flux assay (Fig. S1B). 2DG inhibition persisted throughout the 6-h treatment period and for a further 7 h after removal of 2DG from the medium (Fig. S1C).

Remarkably, 2DG-mediated inhibition of glycolysis reversed the pro-metastatic capabilities initially observed with TAM-sups (Fig. 6). HUVEC network formation was inhibited in TAM-supported networks, as shown by decreases in total network length, total branch points, and total loops, along with an increase in the total number of nets, whereas HPNE-supported network formation was unaffected (Fig. 6A, B). A significant reduction in tumor cell extravasation was also observed in the presence of 2DG-treated TAM-sups but not in the presence of HPNE mac-sup (Fig. 6C). Indicators of EMT were also reversed, as shown by a decrease in the internuclear distance between HPAF-II colonies (Fig. 6D, E), restoration of E-cadherin expression (Fig. 6F), reduced polymerizing F-actin mean intensity, and a decrease in HPAF-II area per cell (Fig. 6G).

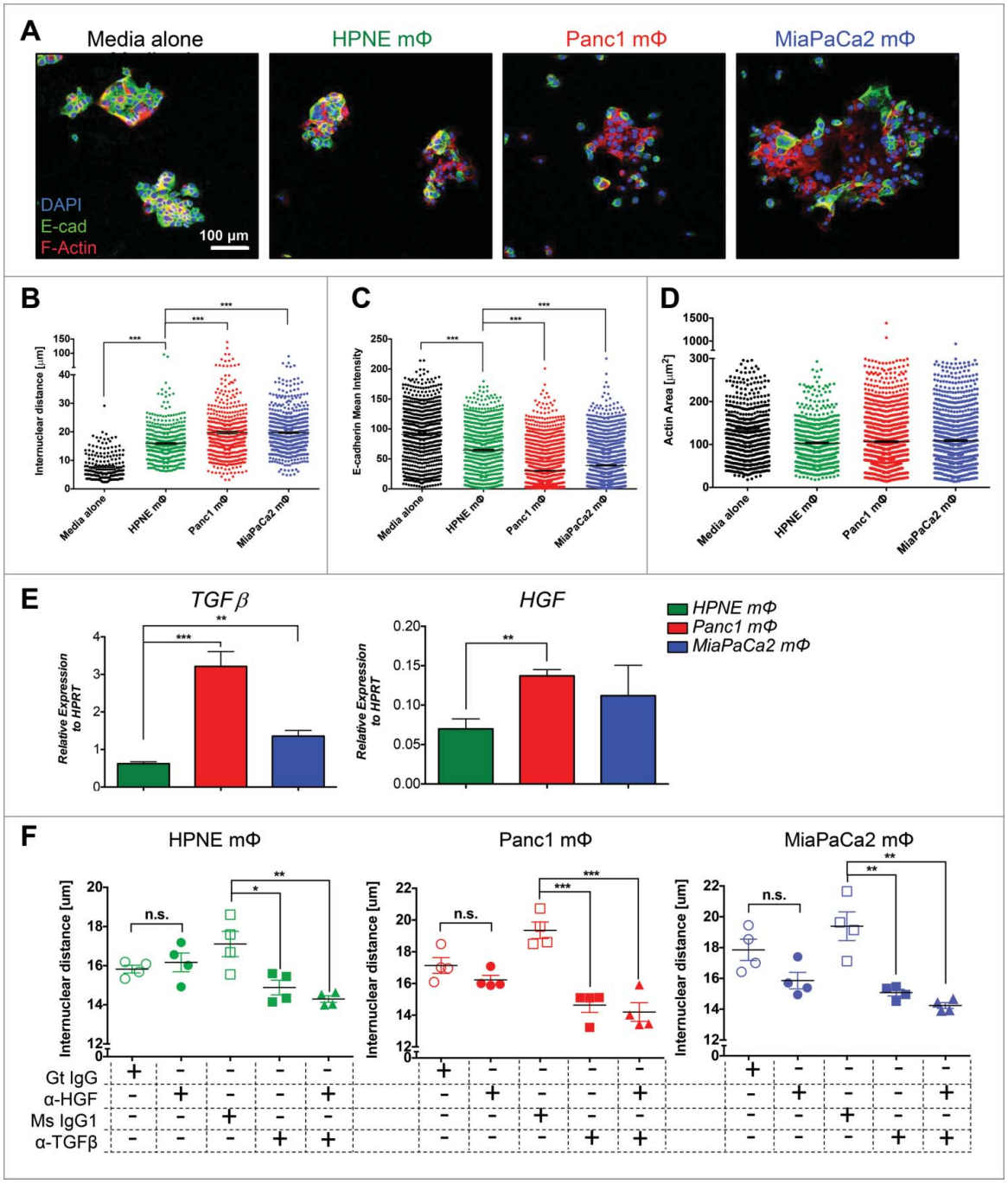

Figure 4. Panc1 and MiaPaCa2 mΦ induced higher rates of EMT compared to HPNE mΦ. 3×10^3 HPAF-II (epithelial pancreatic tumor cell line) cells in single cell suspension were seeded per well in 96-well optical bottom plates and allowed to grow into tight self-contained colonies for 4 d. On day 4, media was aspirated from wells and mΦ supernatants were added to the HPAF-II colonies to induce EMT. After 36–48 h, HPAF-II colonies were assayed by confocal microscopy to determine three key parameters : (i) colony spreading (increase in internuclear distance of neighboring cells within each colony), (ii) loss of epithelial marker (E-cadherin) expression, (iii) morphological "flattening" of cells (increase in area) (A) The representative immunofluorescence images of HPAF-II colonies incubated with the respective mΦ supernatants, stained with E-cadherin and phalloidin are shown. (B) A collated scatter plot of mean ± SEM of the internuclear distance is shown. Each dot represents a measurement between two neighboring HPAF-II cells. (C, D) The collated scatter plots of mean ± SEM of the intensity of E-cadherin (C) and area of F-actin (D) where each dot represent a single HPAF-II cell are shown. (B–D) Data for scatter plots were tabulated from TissueQuest-analyzed images of at least eight colonies per condition. Data are representative of n = 8 (A–D) independent experiments. (E) The bar graphs of mean ± SEM of the transcript expression of TGFβ and HGF of the macrophages by qPCR are shown. Data are representative of n = 3 independent experiments. (F) The collated scatter plots of the mean ± SEM of the internuclear distance from n = 4 independent experiments are shown, in which HGF was neutralized with an anti-HGF antibody (Goat IgG as isotype control), and TGFβ was neutralized with an anti-TGFβ antibody (Mouse IgG1 as isotype control) in the macrophage supernatants. $^{*}p < 0.05$; $^{**}p < 0.01$; $^{***}p < 0.001$; *ns = not significant*.

2DG has been reported to induce ER stress.[23] To rule out the possibility that ER stress induced by 2DG affected the pro-metastatic capabilities of the TAMs, we supplemented 2DG-treated macrophages with exogenous mannose. We observed that mannose supplementation did not affect loop formation in angiogenesis assays (Fig. S2A), or significantly affect HPAF-II colony spreading in EMT assays (Fig. S2B), compared to 2DG alone. Taken together, these results demonstrate that 2DG inhibition of pro-metastatic capabilities of TAMs is a direct result of diminished glycolysis, and not due to downstream effects of ER stress.

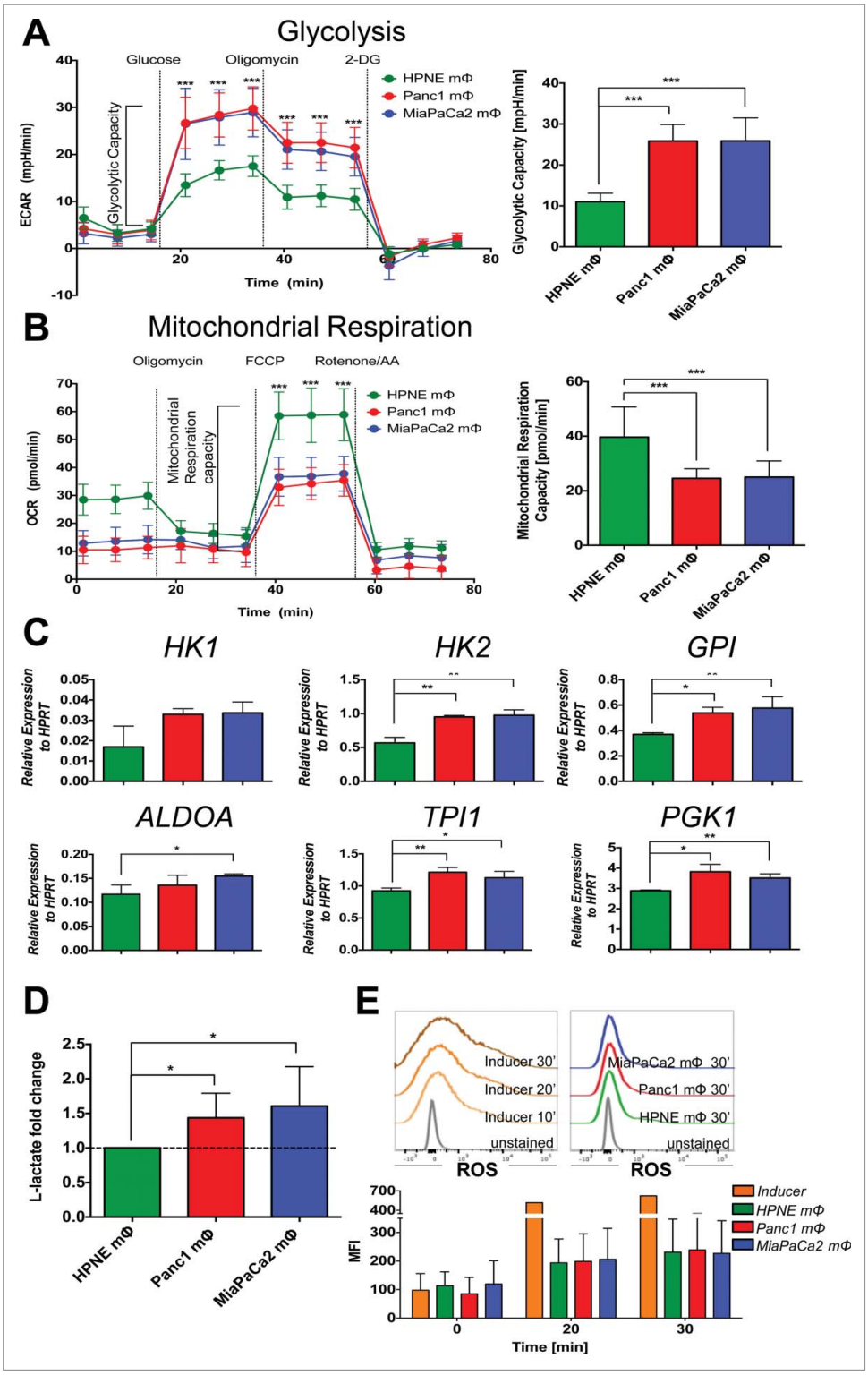

Figure 5. Panc1 and MiaPaCa2 mΦ exhibit pronounced glycolytic profile compared to HPNE mΦ. The representative line graphs of the mean ± SEM of ECAR (A) and OCR (B) values at each timepoint in the Glycolysis Stress test and Mitostress test, respectively, performed on the three mΦ types are shown. Beside the line graphs are bar graphs of the mean ± SEM of calculated glycolytic capacity (A) and maximal mitochondrial respiration capacity (B). Data are representative of n = 9 independent experiments. (C) MΦ are assayed for transcript expression of key glycolysis genes *HK1*, *HK2*, *GPI*, *ALDOA*, *TPI1* and *PGK1* by qPCR. Bar graphs shown are the mean ± SEM of the relative expression of that gene over HPRT. Data are representative of n = 4 independent experiments. (D) A bar graph of the mean ± SEM of the fold change of L-lactate measured by LC-MS of the Panc1 and MiaPaCa2 MΦ lysates with respect to HPNE MΦ lysates is shown. Data is collated from n = 4 independent experiments. (E) The histograms of ROS production, from mΦ induced with a known ROS inducer as a positive control (left panel) and from the three mΦ types at basal level (right panel) are shown. Bar graph below shows the mean ± SEM of ROS MFI collated from n = 2 independent experiments. $^{*}p < 0.05$; $^{**}p < 0.01$;$^{***}p < 0.001$.

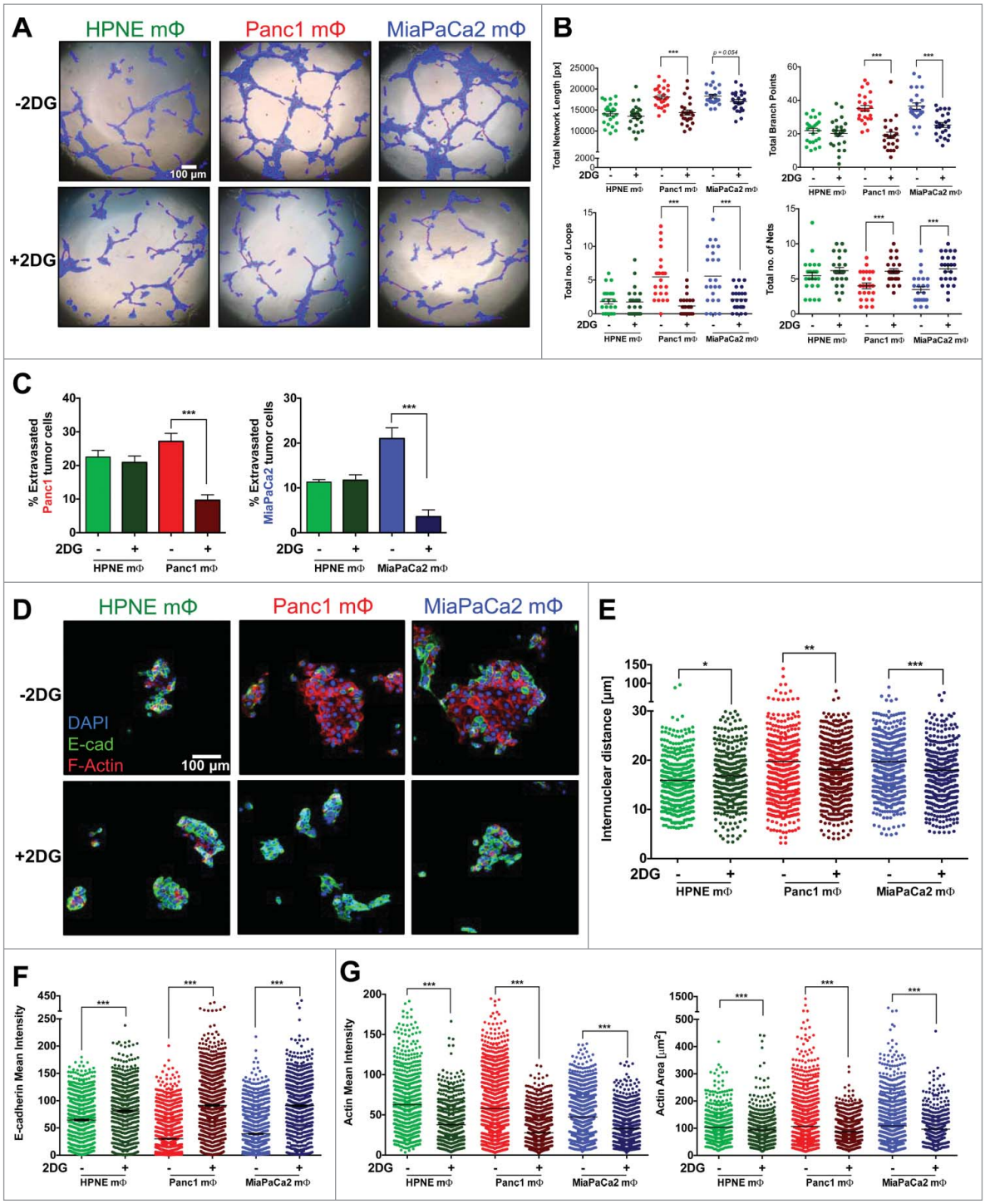

Figure 6. 2DG inhibition of glycolysis in Panc1 and MiaPaCa2 mΦ reverses pro-metastatic phenotype. After 7–9 d of monocytes co-cultured with HPNE, Panc1 and MiaPaCa2 conditioned media to obtain the three mΦ types, media was aspirated and replaced with fresh media with or without 25 mM 2DG for the next 6 h. MΦ supernatants were then harvested and used for downstream angiogenesis (A, B), extravasation (C) and EMT (D–G) assays. (A) The representative bright-field images of HUVEC networks analyzed by Ibidi's WimTube Image Analysis software are shown, along with (B) scatter plots of the mean ± SEM of the key metrics as described in Fig. 2. Data shown is collated from n = 6 independent experiments. (C) The bar graphs of the mean ± SEM of the percentage of extravasated cancer cells, using collated data from at least four devices per condition are shown. $^{***}p < 0.001$. (D) The representative immunofluorescence images of HPAF-II colonies incubated with the respective mΦ supernatants, stained with E-cadherin and phalloidin are shown. (E–G) The scatter plots of the mean ± SEM of internuclear distance (E), mean intensity of E-cadherin (F) and F-actin (G) and the area of F-actin (G) are shown. (E–G) Scatter plots are data of one experiment from at least eight colonies per condition. Data are representative of n = 6 independent experiments.

Given that 2DG can abrogate the pro-metastatic capacities of TAMs, we hypothesized that the reciprocal experiment—an upregulation of glycolysis in the TAMs—could further promote these capacities. We induced glycolysis transiently by overexpressing HK2 (Fig. S3) and GLUT1 (data not shown) by mRNA electroporation and plasmid DNA transfection. Despite clear upregulation of *HK2* transcript expression by qPCR (Fig. S3B), this does not translate to functional upregulation of

glycolysis in live metabolic flux assays (Fig. S3A) or of key glycolytic genes by qPCR (Fig. S3C).

Taken together, these results strongly indicate that the pro-metastatic phenotype of TAMs is dependent on a metabolic commitment to high rates of glycolysis to fulfill such functional requirements, and that inhibition of glycolysis can subvert their pro-metastatic capacities almost entirely.

Discussion

It is increasingly appreciated that tumor cells undergo pronounced metabolic reprogramming to fulfill their bioenergetic and biosynthetic demands in an ongoing effort to support rapid proliferation.[24] Indeed, metabolic reprogramming has recently acquired status as a core hallmark of cancer progression.[25] One of the earliest signs of such profound metabolic changes is the Warburg effect, a phenomenon in which tumor cells almost exclusively use glycolysis to generate energy, even under aerobic conditions.[24] Indeed, these metabolic alterations form the basis for the use of ^{18}Fluoro-Deoxyglucose Positron-Emission Tomography (^{18}FDG-PET) to image and visualize growing tumors in the human body.

The tumor microenvironment is made up of a heterogeneous population of cells in the tumor stroma, including immune cell infiltrates. Macrophages have emerged as key players involved in altering tumor progression and metastasis, and a growing body of evidence indicates that these immune cells are themselves capable of adopting specific metabolic signatures for effector function.[26] However, whether tumor-infiltrating macrophages exhibit the type of metabolic reprogramming reminiscent of tumor cells, and how this, in turn, affects tumor outcomes remains to be elucidated. Here, we show, for the first time in the context of pancreatic cancer, that human *in-vitro*-derived TAMs utilize Warburg metabolism to promote tumor growth and dissemination.

In a model of our summarized findings (illustrated in Fig. 7), we propose that macrophages infiltrating tumor lesions in a chronic "smoldering inflammation" response [27] promote angiogenesis and augment extravasation of tumor cells out of blood vessels in a VEGF-dependent manner. In addition, these TAMs induce EMT, facilitating tumor dissemination to secondary sites, such as the lung and liver, in a TGFβ-dependent manner. This pro-metastatic phenotype correlates with high rates of glycolysis characteristic of the Warburg metabolism. Inhibiting glycolysis in the TAMs using 2DG, a specific inhibitor of HK2, results in significant reversal of all three pro-metastatic capabilities. To our knowledge, our results represent the first direct proof-of-concept that alterations in macrophage metabolism can promote tumor dissemination.

Characterization of our *in-vitro*-generated macrophages revealed that Panc1 and MiaPaCa2 macrophages exhibit a mixed M1 and M2 phenotype,[28] with increased expression of the M2 markers, CD163 and CD206, as well as increased expression of the inflammatory cytokines, IL-1β, IL-6, and TNF-α. This is not surprising, as tumor-infiltrating macrophages are known to be heterogeneous in terms of polarization, location, and function.[29] Indeed, Helm and colleagues also report that freshly isolated TAMs from human PDAC lesions express both M1 (HLA-DR, IL-1β, and TNF-α) and M2 (CD163 and IL-10) markers.[30]

We observed consistently higher rates of glycolysis in TAMs compared with controls, which is in line with findings in the

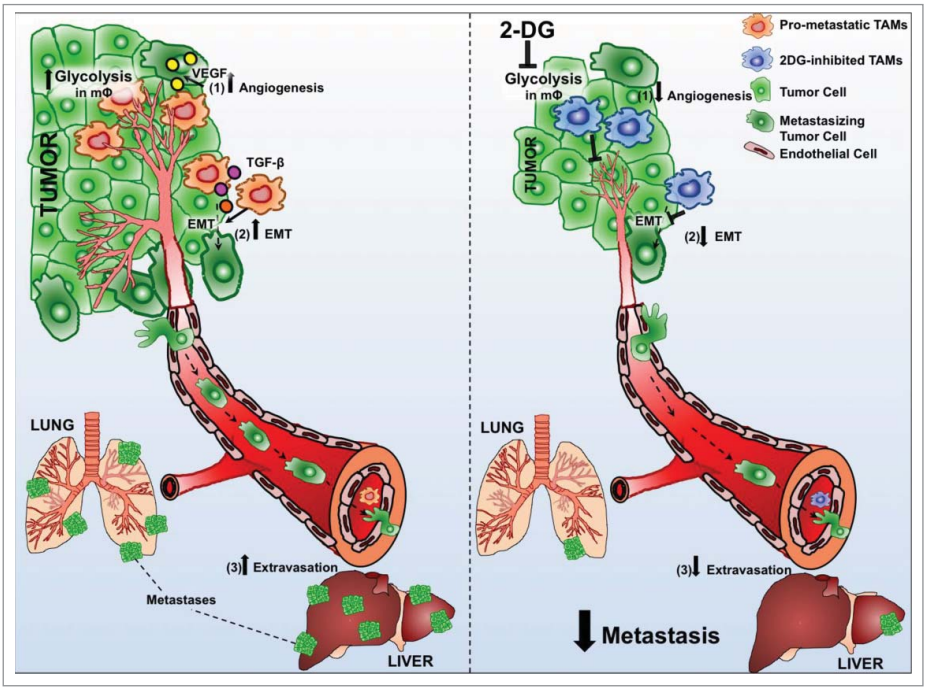

Figure 7. TAMs support metastatic dissemination and colonization at secondary sites. MΦ that infiltrate PDAC lesions adopt a metabolic profile reminiscent of the Warburg effect for which PDAC tumor cells also exhibit.[50] These infiltrating mΦ support tumor cell dissemination by promoting (1) angiogenesis, inducing (2) EMT and augmenting (3) extravasation of tumor cells to potential secondary sites. Sustained inhibition of such high rates of glycolysis using 2DG in TAMs subverts all three pro-metastatic capacities. Taken together, our results highlight the potential of pharmacologics targeted at modulating metabolic pathways that deliver a one–two punch to both immune cells and tumor cells, thus refining our approach to curtailing metastasis in PDAC.

setting of obesity-induced inflammation, which frequently draws parallels to the chronic smoldering inflammation state in tumors. Freemerman and colleagues demonstrated that in mice fed a high-fat diet, macrophages found in crown-like structures and inflammatory foci stained positive for GLUT1, suggesting a connection between increased glucose uptake and a hyperinflammatory state.[31] In addition, stable overexpression of GLUT1 in the RAW264.7 mouse macrophage cell line led to elevated secretion of inflammatory mediators.[31] Several other studies have also reported a link between key glycolytic enzymes and an M1, or LPS-activated macrophage phenotype.[8,9,11,32] Thus, recent evidence supports the notion that upregulation of glycolysis in macrophages confers a pro-inflammatory phenotype.

The transcription factor Hypoxia-inducible factor 1 α (HIF1α), which is upregulated during glycolysis, also activates the transcription of VEGF,[33] providing a connection between increased glycolysis in TAMs to its ability to promote angiogenesis. Although we could detect VEGFA by qPCR in all three macrophage types, VEGFA was barely detected at the protein level in the macrophage supernatants, as were several other angiogenesis-associated factors such as Angiogenin, Angiopoietin-1, -2 etc. (data not shown). This suggests that in addition to VEGF, a combination of other factors could together be promoting angiogenesis.

While there is currently little evidence describing how glycolysis directly affects TGFβ signaling, activation of this pathway in breast-cancer-associated fibroblasts has been reported to increase oxidative stress and glycolysis in these stromal cells,[34] suggesting a connection between TGFβ signaling and glucose metabolism. Indeed, we observed that 2DG inhibition resulted in a 2- to 3-fold reduction in transcript expression of TGFβ in TAMs (data not shown). Taken together, our results are consistent with existing literature linking VEGF and TGFβ to enhanced glucose metabolism.

In our hands, we were unable to increase glycolytic rates of our *in-vitro*-conditioned macrophages further after glucose addition, despite trying several approaches such as HK2/GLUT1 overexpression and using drugs that target the ETC such as oligomycin, metformin, phenformin and rotenone (latter three, data not shown). Oligomycin, used as a positive control in the Glycolysis Stress Test to shift energy production from OXHPOS to glycolysis and reveal the maximum glycolytic capacity of the cells, invariably failed to upregulate glycolysis in these macrophages (Fig. 5; Fig. S1B and S3A, 2nd stage of Glycolysis Stress Test). We hypothesize that in these *in-vitro*-conditioned macrophages, induction of glycolysis have possibly reached a functional maximum and could not be further increased.

Others have shown that overexpression of signaling mediators in myeloid cells, such as Akt in mouse bone-marrow-derived dendritic cells[35] and CARKL in the mouse RAW264.7 macrophage cell line,[7] are able to sustain induction of glycolysis. However, to our knowledge, there are no reports thus far in primary myeloid cells demonstrating the effects of induction of glycolysis on functional polarization. We observed that incubation with 2DG for longer than 8 h results in over 50% cell death in our macrophage populations (data not shown), suggesting that these cells may be sensitive to such prolonged metabolic changes. It has also been reported that HK2 overexpression in cardiomyocyte and noncardiomyocyte cells induces autophagy in glucose-limiting conditions.[36] Thus, macrophages may also display resistance to upregulation of glycolysis as a compensatory mechanism to prevent autophagy and conserve energy resources.

Apart from glucose metabolism, it is possible that other types of metabolic programs involved in macrophage polarization may also be utilized in our *in-vitro*-generated TAMs. M1 and M2 polarization has been related to distinct metabolic characteristics pertaining to lipid and iron metabolism.[29,37,38] Similarly, reprogramming in glucose and amino acid metabolism was reported for dendritic cells and T cells upon activation.[26,39] Indeed, there is accumulating evidence for global metabolic changes in immune cells in the context of cancer.[40] In PDAC, a new study by Son and colleagues has recently shown that PDAC tumor cells are highly dependent on a glutamine-based series of reactions to support tumorigenic growth.[41] Whether this glutamine "addiction," or other types of lipid, iron, or amino acid metabolism, is preferentially utilized by tumor-infiltrating macrophages remains to be explored.

A number of other unanswered questions remain. Which factors in Panc1 and MiaPaca2 tumor-conditioned media differentiate it from HPNE normal-conditioned media? Deconvolution of tumor-conditioned media is required to elucidate which growth factors or cytokines are responsible for promoting the pro-metastatic phenotype observed. The signaling pathways downstream of glycolysis that mediate the pro-metastatic phenotype in these TAMs are also unknown. Prevailing evidence in other immune cell types suggest a variety of possibilities. PI3K/Akt,[35] mTOR,[42] AMPK,[42] and the Nlrp3 inflammasome[43] have all been shown to mediate downstream signaling pathways upon nutrient-sensing. Incio and colleagues report that activating AMPK signaling pathways with metformin is able to reduce the M2 markers Arg1 and IL-10 in TAMs isolated from orthotopic models of mouse PDAC.[44] This is associated with an alleviation of desmoplasia at the tumor site, and reduction of both EMT and systemic metastasis.[44] These results point toward possible AMPK signaling in Panc1 and MiaPaCa2-TAMs. However, detailed exploration into the signaling pathways involved in these TAMs is beyond the scope of this study.

Finally, do our findings extend to other cancers? In unrelated, currently unpublished studies, other investigators have found evidence for Warburg metabolism in myeloid cells in the context of mouse ovarian and human renal and thyroid carcinomas, indicating that our observations are not restricted to the setting of PDAC (personal communication).

Taken together, our results suggest that targeting metabolic pathways in immune cells, such as macrophages, represents a potential strategy to keep tumor metastasis in check. Modulating glycolysis to reshape the immune response in the context of cancer is not without precedent. A recent report by Chang and colleagues demonstrated in a mouse sarcoma model that enhancing tumor cell glycolysis in an antigenic "regressor" tumor is sufficient to override the cytotoxic ability of T cells to destroy tumor cells in an IFNγ-dependent manner.[45]

Since all tumor cells are dependent on metabolic reprogramming to maintain growth and survival, targeting metabolism

raises the possibility of affecting cancers arising from diverse tissue types. Indeed, the enzyme L-asparaginase has been used to treat acute lymphoblastic leukemia (ALL) and related lymphomas,[46] thus illustrating how the distinct metabolism of tumor cells can be successfully exploited for cancer therapy.

Because normal proliferating cells have the same metabolic needs as cancer cells, it will be essential to determine an appropriate therapeutic window, which is clinically useful while still ensuring safety.[46] Despite these challenges, the burgeoning field of immunometabolism has renewed interest in the exploration of metabolic enzymes as viable pharmacological targets to deliver a simultaneous hit to both tumor and pro-metastatic immune cells.

Materials and methods

Generation of conditioned media

Conditioned media were generated from a normal pancreatic epithelial cell line hTERT-HPNE ("HPNE") (ATCC® CRL-4023) and the PDAC epithelial cell lines Panc1 (ATCC® CRL-1469) and MiaPaCa2 (ATCC® CRL-1420). Cells were seeded at the same cell density, 1×10^6 cells in 30 mL of complete IMDM ("cIMDM," IMDM supplemented with 5% Human serum and 1× Penicillin-Streptomycin) in a T175 flask, and grown to 70–80% confluency. The conditioned media was then removed from the flasks, centrifuged for 10 min at 1500 rpm, sterile-filtered (0.2 μm), aliquoted, and stored at −20°C.

Development of in vitro-generated TAMs

All blood samples used in this study were approved by the Institutional Review Board, Singapore in accordance to guidelines of the Health Science Authority of Singapore (Reference code: NUS-IRB10-250). Peripheral blood mononuclear cells (PBMCs) were obtained from blood of healthy donors using Ficoll density centrifugation. Monocytes were isolated with α-CD14-conjugated microbeads by magnetic-automated cell sorting (MACS) (Miltenyi Biotec), and cultured with conditioned media (thawed and warmed to 37°C) for 7–9 d. Each donor represents one independent experiment. Macrophages generated using these conditioned media were then assayed to verify the differentiation of *bona fide* macrophages. For macrophage supernatant experiments, the conditioned media were removed from the mature HPNE−, Panc1−, and MiaPaCa2− macrophages after the 7–9-d culture, and replaced with fresh cIMDM for 6 h. This media was then harvested and used as macrophage supernatant (labeled mac-sup or TAM-sup as detailed in the *Results* section).

Flow cytometry

Macrophages were resuspended in FACS buffer (10% Fetal calf serum, 5% Human serum, 0.01% sodium azide in PBS). After Fc blockade with anti-FcγRIII/II (BD Biosciences), cells were stained with DAPI, and surface-stained with anti-CD163 APC (BioLegend 333610), anti-CD206 APC-Cy7 (BioLegend 321120), and M-CSFR PE (BioLegend 347304). Intracellular CD68 was stained using anti-CD68 Alexa 488 (BioLegend 333811) as per the manufacturer's instructions. Annexin-V APC (eBiosciences 88-8007) was stained as per the manufacturer's instructions. Flow cytometric analysis was performed on a BD Fortessa flow cytometer (BD Biosciences).

Endocytosis assay

Macrophages were harvested by gentle scraping, and washed with warm cIMDM three times prior to incubation with 100 μg/mL of pHrodo-red Dextran beads (Invitrogen) in cIMDM at 37°C for 2 or 20 min. The macrophages were washed again with warm cIMDM three times and immediately assayed for pHrodo-red Dextran uptake by flow cytometry. pHrodo-Red dextran has a pH-sensitive fluorescence emission that increases in intensity with increasing acidity, and thus acts as an indicator of active endocytosis.

RT-qPCR

Cells were lysed with Qiazol (Qiagen), and total RNA was purified using the RNeasy Mini kit (Qiagen), as per the manufacturer's instructions. DNase-treated total RNA (0.5–1 μg) was reverse-transcribed to cDNA using iScript Reverse Transcription Supermix (Bio-Rad). Expression of *IL-1β*, *IL-6*, *TNFα*, *CCL3*, *IL-10*, *Arg1*, *HK1*, *HK2*, *GPI*, *ALDOA*, *TPI1*, *PGK1*, *HIF1α*, *LDHA*, *VEGFA*, *TGF-β*, and *HGF* were determined by quantitative PCR with KAPA Sybr FAST ABI Prism 2× qPCR Master Mix (KAPA Biosystems) as per the manufacturer's instructions using an ABI 7900HT Fast Real-Time PCR System (Applied Biosystems). Levels of the housekeeping gene *HPRT* were measured in a separate reaction, and used to normalize the data. List of qPCR primer sequences are listed in Table S1.

HUVEC network formation assay

HUVECs were grown in EndoGRO-LS media (Millipore) to 60–80% confluency before harvesting. EC Matrix (Millipore), a form of matrigel, was thawed on ice and left at 4°C overnight prior to use. On the day of assay, 10 μL of EC Matrix was added to the inner well of a μ-angiogenesis slide (Ibidi) and allowed to solidify at 37°C for at least 3 h. HUVECs (1×10^4) in 20 μL of EndoGRO-LS media were seeded into the upper well of the μ-angiogenesis slide together with 20 μL of macrophage supernatant. HUVEC networks were allowed to form over the next 6 h at 37°C before termination of the assay. VEGF-A (200 ng/mL) and the VEGFR inhibitor Sorafenib (10 μM) were used as positive and negative controls, respectively. Network formation was captured by bright-field imaging using an Olympus epifluorescent microscope at the 4-h timepoint. At least four non-overlapping images were captured at 10× magnification per well. Images were quantitatively analyzed with WimTube software (Ibidi) to evaluate key network formation metrics, such as total network length, total number of branching points, loops, and nets. Following WimTube metrics, a segment is considered to be part of the segmental structure between two branching points, or a branching point and a loose end (identified by red lines in the bright-field images of Figs. 2A and 6A). Total network length refers to the total number of segments multiplied by the individual segment length in

pixels (identified by blue regions in the bright-field images of Figs. 2A and 6A). Branching points refer to parts of the skeleton where three or more segments converge/diverge. A loop refers to an area of the background enclosed (or almost enclosed) by the segmental structures. A net refers to an isolated region of segments that contains at least one branching point; thus, isolated segments are not considered nets. A net is essentially an incomplete loop, and is inversely proportional to loop formation.

Extravasation assay

The microfluidic device consists of a polydimethylsiloxane (PDMS) layer bonded to a glass coverslip by plasma treatment to form a central gel region and two adjacent fluidic channels. The PDMS replica was fabricated by soft lithography and a poly-d-lysine (PDL) coating of the microchannels was applied to improve the hydrogel attachment to the channel walls as previously described.[47] Each of the three channels has a width of 1 mm, a height of 120 μm, and the central gel region is in contact for about 9 mm in length with the two lateral fluidic channels. To create the three-dimensional matrix, a type-I collagen gel solution (2.5 mg/mL, pH 7.4) was injected into the central region and polymerized at 37°C for 30 min. GFP-HUVECs (5×10^6 cells/mL) in 50 μL of EGM-2 media (Lonza) were seeded in one of the fluidic channels pre-coated with 50 μg/mL fibronectin. After 3 d, a uniform monolayer covering the four walls of the channel was formed mimicking a blood vessel. Panc1 and MiaPaCa2 tumor cells, with or without macrophages, were injected in the same microchannel to investigate their extravasation across the endothelial monolayer into the gel region. Tumor cells and macrophages were seeded at a ratio of 1:1 with a concentration of 1.5×10^5 cells/mL for each cell type in EGM-2 media. Macrophages and pancreatic cells were labeled prior to seeding into the device. Macrophages were stained with Vybrant DiD (Life Technologies) live cell-labeling solution, while pancreatic cells were labeled with PKH26 Red Fluorescent Cell Linker for Cell Membrane (Sigma-Aldrich). Nuc Blue Live Cell Stain for Nucleus (Life Technologies) was used for both macrophages and tumor cells. For the experiments using macrophage supernatants only, the tumor cells were resuspended in the macrophage supernatants, and injected into the device as described before. After 24 h, the devices were fixed with 4% paraformaldehyde (PFA) for 12 min, washed, and stored at 4°C before confocal imaging. The images were captured using an Olympus IX81 confocal microscope. Images were analyzed with IMARIS software (Bitplane Scientific Software) to quantify the extravasation of pancreatic cells under the different test conditions. The number of extravasated tumor cells was counted and expressed as a percentage of the total number of cells present on the monolayer.

EMT assay

Pancreatic epithelial tumor cell line HPAF-II (EMT score = −0.556) (ATCC CRL-1997) was seeded at 3×10^3 cells per well in 200 μL of cIMDM in Nunc MicroWell 96-Wwell black-wall optical-bottom plates. After 4 d, HPAF-II colonies were in tight self-contained colonies, approximately 10–20 cells in size. Media was aspirated from the wells before addition of macrophage supernatants and EMT-inducing media (a gift from R&D Systems, CCM017) at a 1:1 ratio. EMT induction was allowed to proceed for 36–48 h before the media was removed and cells were fixed with 4% PFA for 30 min at 4°C. The wells were washed with PBS twice and blocked with 10% normal goat serum for 10 min before staining with mouse monoclonal anti-human E-cadherin (BD Biosciences 610182) and Alexa Fluor 647-conjugated phalloidin (Life Technologies A22287). After three washes of PBS, the cells were stained with donkey anti-mouse Alexa Fluor 488 (ThermoFisher Scientific R37114). Cells were washed with PBS three times and stained with DAPI for 5 min. PBS (100 μL) was added to each well and plates were stored at 4°C before imaging. HPAF-II colonies were imaged using an FV-1000 confocal system with an inverted Olympus IX81 microscope. Internuclear distance was calculated using DAPI alone images ran on an in-house script to determine closest distance between two adjacent nuclei. To plot the mean intensity and area of E-cadherin and actin, images were analyzed by TissueQuest software (TissueGnostics).

Live metabolic flux assay

The mitochondria oxygen consumption rate (OCR, O_2 pmol/min) and extracellular acidification rate (ECAR, mpH/min) of macrophages were analyzed using an XF^{e}96 extracellular flux analyzer (Seahorse Bioscience) according to the manufacturer's instructions. For the Glycolysis Stress Test ECAR analysis, macrophages were harvested, washed, and resuspended in ECAR medium (DMEM base [no bicarbonate] with 2 mM L-glutamine, 143 mM NaCl, and 0.5% phenol red [pH 7.35]). This test consisted of four consecutive stages: basal (without drugs), glycolysis induction (10 mM glucose), maximal glycolysis induction (5 μM oligomycin), and glycolysis inhibition (100 mM 2DG). Glycolytic capacity was calculated as follows: (Mean of highest ECAR values induced by glucose or oligomycin) – (Mean of basal ECAR values). For the Mito Stress Test OCR analysis, macrophages were harvested, washed, and resuspended in OCR medium (DMEM base, 25 mM glucose, 1 mM pyruvate, 2 mM L-glutamine [pH 7.35]). This test also consisted of four consecutive stages: basal respiration (without drugs), mitochondrial complex V inhibition (5 μM oligomycin), maximal respiration induction (5 μM carbonyl cyanide 4-(trifluoromethoxy) phenylhydrazone (FCCP)), and electron transport chain inhibition (1 μM rotenone and 1 μM antimycin A). Mitochondrial respiration capacity was calculated as follows: (Mean of highest OCR values induced by FCCP) – (Mean of OCR values after oligomycin addition). Macrophages were resuspended in the respective media were and seeded at 8×10^4/well in flat-bottom 96-well Seahorse Microculture plates, and incubated in a non-CO_2 incubator for 1 h at 37°C prior to the start of each assay.

Metabolomics analysis

Metabolites from 5×10^6 macrophages of each phenotype were extracted based on a two-phase liquid extraction protocol and subsequently analyzed using reverse phase liquid chromatography, in tandem with high-resolution mass spectrometry as

previously described.[48] Data pre-processing was performed using an in-house software incorporating the XCMS peak finding algorithm[49] and differential metabolites with p values less than 0.05 (Student's t-test with Welch correction) were identified.

Inhibition and overexpression of HK2

To inhibit glycolysis in the fully conditioned macrophages (after 7–9 d of incubation in conditioned media), media was removed and replaced with fresh cIMDM with or without 2DG, a competitive inhibitor of HK2, to a final concentration of 25 mM for 6 h at 37°C. In some experiments, 5 mM mannose was supplemented to 2DG-treated wells for the same time period. To promote glycolysis, HK2 was overexpressed by transfection with an HK2 plasmid (Origene SC309063). Fully conditioned macrophages were harvested and re-plated at 0.8×10^6 cells/well in 900 μL of Opti-MEM media (Gibco) in a 12-well plate and allowed to re-adhere to the well surface for 30 min. Purified HK2 plasmid DNA (1.25 μg) was pre-incubated with 7.5 μL of Lipofectamine 2000 (Life Technologies) in 100 μL of Opti-MEM for 5 min at room temperature before adding to the macrophages for 6 h at 37°C. Mock transfections were set up without DNA. Inhibition and induction of glycolysis was determined using live metabolic flux assays and RT-qPCR.

Reactive oxygen species (ROS) production

ROS was measured using 1 μM of Oxidative Stress Detection Reagent from the total Reactive Oxygen Species/SuperOxide detection kit (Enzo LifeSciences ENZ-51010) according to the manufacturer's instructions. Macrophages were incubated with the oxidative stress detection reagent for 0, 10, 20, and 30 min, and analyzed using a BD Fortessa (BD Biosciences). Pyocyanin (100 μM) was used as a positive control to induce ROS.

Neutralization of VEGF, HGF and TGFβ

0.2 μg/mL anti-VEGFA-neutralizing antibody (R&D AF-293-NA) was incubated along with the macrophage supernatants in angiogenesis assays as indicated. 20 μg/mL anti-HGF neutralizing antibody (Abcam ab10679) and 50 μg/mL anti-TGFβ neutralizing antibody (eBiosciences 16-9243) were incubated along with macrophage supernatants in EMT assays, where indicated.

Disclosure of potential conflicts of interest

No potential conflicts of interest were disclosed.

Acknowledgments

We thank the Singapore Health Sciences Authority Blood bank for apheresis cone donors. We thank Professor Seok Chung (Korea University) for the microfluidic device design. We thank Shu Wen Chen for performing the lipid profiling in the metabolomics experiments, the results of which we did not include in this manuscript. We also thank Kerry McLaughlin of Insight Editing London for critical evaluation of the manuscript prior to publication.

Funding

This work was funded by the Biomedical Research Council (BMRC), A*STAR and by the Singapore-MIT Alliance for Research and Technology (SMART – BioSym IRG).

Author contributions

H.L.P. conceived, designed, performed, analyzed, interpreted all experiments, and wrote the manuscript. J.L.S., W.H.Y., P.S., B.S.L. assisted with experimental work and analyzed data. G.A. designed, performed, and interpreted all the extravasation experiments, analyzed data, and wrote the parts in the manuscript relevant to extravasation. B.L. and T.L. analyzed data. Y.S.H. and S.Y.M. performed the metabolomics experiments. C.K.O. provided material support. R.Y.H. assisted with the development of methodology. O.R., R.D.K., and F.G. reviewed the manuscript. S.C.W. supervised the project, analyzed, interpreted data, and wrote the manuscript.

References

1. Bardeesy N, DePinho RA. Pancreatic cancer biology and genetics. Nat Rev Cancer 2002; 2:897-909; PMID:12459728; http://dx.doi.org/10.1038/nrc949
2. Rhim Andrew D, Mirek Emily T, Aiello Nicole M, Maitra A, Bailey Jennifer M, McAllister F, Reichert M, Beatty Gregory L, Rustgi Anil K, Vonderheide Robert H et al. EMT and dissemination precede pancreatic tumor formation. Cell 2012; 148:349-61; PMID:22265420; http://dx.doi.org/10.1016/j.cell.2011.11.025
3. Qian B-Z, Pollard JW. Macrophage diversity enhances tumor progression and metastasis. Cell 2010; 141:39-51; PMID:20371344; http://dx.doi.org/10.1016/j.cell.2010.03.014
4. Qian B, Deng Y, Im JH, Muschel RJ, Zou Y, Li J, Lang RA, Pollard JW. A distinct macrophage population mediates metastatic breast cancer cell extravasation, establishment and growth. PLoS One 2009; 4:e6562; PMID:19668347; http://dx.doi.org/10.1371/journal.pone.0006562
5. Kitamura T, Qian B-Z, Soong D, Cassetta L, Noy R, Sugano G, Kato Y, Li J, Pollard JW. CCL2-induced chemokine cascade promotes breast cancer metastasis by enhancing retention of metastasis-associated macrophages. J Exp Med 2015; 212:1043-59; PMID:26056232; http://dx.doi.org/10.1084/jem.20141836
6. Le A, Cooper CR, Gouw AM, Dinavahi R, Maitra A, Deck LM, Royer RE, Vander Jagt DL, Semenza GL, Dang CV. Inhibition of lactate dehydrogenase A induces oxidative stress and inhibits tumor progression. Proc Natl Acad Sci 2010; 107:2037-42; PMID:20133848; http://dx.doi.org/10.1073/pnas.0914433107
7. Haschemi A, Kosma P, Gille L, Evans Charles R, Burant Charles F, Starkl P, Knapp B, Haas R, Schmid Johannes A, Jandl C et al. The sedoheptulose kinase CARKL directs macrophage polarization through control of glucose metabolism. Cell Metab 2012; 15:813-26; PMID:22682222; http://dx.doi.org/10.1016/j.cmet.2012.04.023
8. Tan Z, Xie N, Cui H, Moellering DR, Abraham E, Thannickal VJ, Liu G. Pyruvate dehydrogenase kinase 1 participates in macrophage polarization via regulating glucose metabolism. J Immunol 2015; 194:6082-9; PMID:25964487; http://dx.doi.org/10.4049/jimmunol.1402469
9. Palsson-McDermott Eva M, Curtis Anne M, Goel G, Lauterbach Mario AR, Sheedy Frederick J, Gleeson Laura E, van den Bosch Mirjam WM, Quinn Susan R, Domingo-Fernandez R, Johnston Daniel GW et al. Pyruvate kinase M2 regulates Hif-1α activity and IL-1β induction and is a critical determinant of the Warburg effect in LPS-activated macrophages. Cell Metab 2015; 21:65-80; PMID:25565206; http://dx.doi.org/10.1016/j.cmet.2014.12.005
10. Tawakol A, Singh P, Mojena M, Pimentel-Santillana M, Emami H, MacNabb M, Rudd JHF, Narula J, Enriquez JA, Través PG et al. HIF-1α and PFKFB3 mediate a tight relationship between proinflammatory activation and anerobic metabolism in atherosclerotic macrophages. Arterioscler Thromb Vasc Biol 2015; 35:1463-71; PMID:25882065; http://dx.doi.org/10.1161/ATVBAHA.115.305551

11. Ruiz-García A, Monsalve E, Novellasdemunt L, Navarro-Sabaté À, Manzano A, Rivero S, Castrillo A, Casado M, Laborda J, Bartrons R et al. Cooperation of adenosine with macrophage toll-4 receptor agonists leads to increased glycolytic flux through the enhanced expression of PFKFB3 Gene. J Biol Chem 2011; 286:19247-58; http://dx.doi.org/10.1074/jbc.M110.190298
12. Lesina M, Kurkowski MU, Ludes K, Rose-John S, Treiber M, Kloppel G, Yoshimura A, Reindl W, Sipos B, Akira S et al. Stat3/Socs3 activation by IL-6 transsignaling promotes progression of pancreatic intraepithelial neoplasia and development of pancreatic cancer. Cancer Cell 2011; 19:456-69; PMID:21481788; http://dx.doi.org/10.1016/j.ccr.2011.03.009
13. Chan JM, Zervantonakis IK, Rimchala T, Polacheck WJ, Whisler J, Kamm RD. Engineering of in vitro 3D capillary beds by self-directed angiogenic sprouting. PLoS One 2012; 7:e50582; PMID:23226527; http://dx.doi.org/10.1371/journal.pone.0050582
14. Lim SH, Kim C, Aref AR, Kamm RD, Raghunath M. Complementary effects of ciclopirox olamine, a prolyl hydroxylase inhibitor and sphingosine 1-phosphate on fibroblasts and endothelial cells in driving capillary sprouting. Integr Biol (Camb) 2013; 5:1474-84; PMID:24190477; http://dx.doi.org/10.1039/c3ib40082d
15. Aref AR, Huang RY, Yu W, Chua KN, Sun W, Tu TY, Bai J, Sim WJ, Zervantonakis IK, Thiery JP et al. Screening therapeutic EMT blocking agents in a three-dimensional microenvironment. Integr Biol (Camb) 2013; 5:381-9; PMID:23172153; http://dx.doi.org/10.1039/c2ib20209c
16. Bai J, Tu TY, Kim C, Thiery JP, Kamm RD. Identification of drugs as single agents or in combination to prevent carcinoma dissemination in a microfluidic 3D environment. Oncotarget 2015; 6:36603-14; PMID:26474384; http://dx.doi.org/10.18632/oncotarget.5464
17. Bai J, Adriani G, Dang TM, Tu TY, Penny HX, Wong SC, Kamm RD, Thiery JP. Contact-dependent carcinoma aggregate dispersion by M2a macrophages via ICAM-1 and beta2 integrin interactions. Oncotarget 2015; 6:25295-307; PMID:26231039; http://dx.doi.org/10.18632/oncotarget.4716
18. Zervantonakis IK, Hughes-Alford SK, Charest JL, Condeelis JS, Gertler FB, Kamm RD. Three-dimensional microfluidic model for tumor cell intravasation and endothelial barrier function. Proc Natl Acad Sci U S A 2012; 109:13515-20; PMID:22869695; http://dx.doi.org/10.1073/pnas.1210182109
19. Bersini S, Jeon JS, Dubini G, Arrigoni C, Chung S, Charest JL, Moretti M, Kamm RD. A microfluidic 3D in vitro model for specificity of breast cancer metastasis to bone. Biomaterials 2014; 35:2454-61; PMID:24388382; http://dx.doi.org/10.1016/j.biomaterials.2013.11.050
20. Chen MB, Whisler JA, Jeon JS, Kamm RD. Mechanisms of tumor cell extravasation in an in vitro microvascular network platform. Integr Biol (Camb) 2013; 5:1262-71; PMID:23995847; http://dx.doi.org/10.1039/c3ib40149a
21. Quail DF, Joyce JA. Microenvironmental regulation of tumor progression and metastasis. Nat Med 2013; 19:1423-37; PMID:24202395; http://dx.doi.org/10.1038/nm.3394
22. Thiery JP, Acloque H, Huang RYJ, Nieto MA. Epithelial-mesenchymal transitions in development and disease. Cell 2009; 139:871-90; PMID:19945376; http://dx.doi.org/10.1016/j.cell.2009.11.007
23. Yu S-M, Kim S-J. Endoplasmic reticulum stress (ER-stress) by 2-deoxy-D-glucose (2DG) reduces cyclooxygenase-2 (COX-2) expression and N-glycosylation and induces a loss of COX-2 activity via a Src kinase-dependent pathway in rabbit articular chondrocytes. Exp Mol Med 2010; 42:777-86; PMID:20926918; http://dx.doi.org/10.3858/emm.2010.42.11.079
24. Ward Patrick S, Thompson Craig B. Metabolic reprogramming: A cancer hallmark even Warburg did not anticipate. Cancer Cell 2012; 21:297-308; PMID:22439925; http://dx.doi.org/10.1016/j.ccr.2012.02.014
25. Hanahan D, Weinberg Robert A. Hallmarks of cancer: the next generation. Cell 2011; 144:646-74; PMID:21376230; http://dx.doi.org/10.1016/j.cell.2011.02.013
26. Pearce Erika L, Pearce Edward J. Metabolic pathways in immune cell activation and quiescence. Immunity 2013; 38:633-43; PMID:23601682; http://dx.doi.org/10.1016/j.immuni.2013.04.005
27. Mantovani A, Allavena P, Sica A, Balkwill F. Cancer-related inflammation. Nature 2008; 454:436-44; PMID:18650914; http://dx.doi.org/10.1038/nature07205
28. Murray Peter J, Allen Judith E, Biswas Subhra K, Fisher Edward A, Gilroy Derek W, Goerdt S, Gordon S, Hamilton John A, Ivashkiv Lionel B, Lawrence T et al. Macrophage activation and polarization: nomenclature and experimental guidelines. Immunity 2014; 41:14-20; PMID:25035950; http://dx.doi.org/10.1016/j.immuni.2014.06.008
29. Biswas SK, Mantovani A. Macrophage plasticity and interaction with lymphocyte subsets: cancer as a paradigm. Nat Immunol 2010; 11:889-96; PMID:20856220; http://dx.doi.org/10.1038/ni.1937
30. Helm O, Held-Feindt J, Grage-Griebenow E, Reiling N, Ungefroren H, Vogel I, Krüger U, Becker T, Ebsen M, Röcken C et al. Tumor-associated macrophages exhibit pro- and anti-inflammatory properties by which they impact on pancreatic tumorigenesis. Int J Cancer 2014; 135:843-61; PMID:24458546; http://dx.doi.org/10.1002/ijc.28736
31. Freemerman AJ, Johnson AR, Sacks GN, Milner JJ, Kirk EL, Troester MA, Macintyre AN, Goraksha-Hicks P, Rathmell JC, Makowski L. Metabolic reprogramming of macrophages: glucose transporter 1 (GLUT1)-mediated glucose metabolism drives a proinflammatory phenotype. J Biol Chem 2014; 289:7884-96; PMID:24492615; http://dx.doi.org/10.1074/jbc.M113.522037
32. Tannahill GM, Curtis AM, Adamik J, Palsson-McDermott EM, McGettrick AF, Goel G, Frezza C, Bernard NJ, Kelly B, Foley NH et al. Succinate is an inflammatory signal that induces IL-1-beta through HIF-1alpha. Nature 2013; 496:238-42; PMID:23535595; http://dx.doi.org/10.1038/nature11986
33. Ferrara N, Davis-Smyth T. The biology of vascular endothelial growth factor. Endocr Rev 1997; 18:4-25; PMID:9034784; http://dx.doi.org/10.1210/edrv.18.1.0287
34. Guido C, Whitaker-Menezes D, Capparelli C, Balliet R, Lin Z, Pestell RG, Howell A, Aquila S, And∫ S, Martinez-Outschoorn U et al. Metabolic reprogramming of cancer-associated fibroblasts by TGF-β drives tumor growth: connecting TGF-β signaling with "Warburg-like" cancer metabolism and L-lactate production. Cell Cycle 2012; 11:3019-35; PMID:22874531; http://dx.doi.org/10.4161/cc.21384
35. Krawczyk CM, Holowka T, Sun J, Blagih J, Amiel E, DeBerardinis RJ, Cross JR, Jung E, Thompson CB, Jones RG et al. Toll-like receptor–induced changes in glycolytic metabolism regulate dendritic cell activation. Blood 2010; 115:4742-9; PMID:20351312; http://dx.doi.org/10.1182/blood-2009-10-249540
36. Roberts David J, Tan-Sah Valerie P, Ding Eric Y, Smith Jeffery M, Miyamoto S. Hexokinase-II positively regulates glucose starvation-induced autophagy through TORC1 Inhibition. Mol Cell 2014; 53:521-33; PMID:24462113; http://dx.doi.org/10.1016/j.molcel.2013.12.019
37. Biswas SK, Mantovani A. Orchestration of metabolism by macrophages. Cell Metab 2012; 15:432-7; PMID:22482726; http://dx.doi.org/10.1016/j.cmet.2011.11.013
38. Jha Abhishek K, Huang Stanley C-C, Sergushichev A, Lampropoulou V, Ivanova Y, Loginicheva E, Chmielewski K, Stewart Kelly M, Ashall J, Everts B et al. Network integration of parallel metabolic and transcriptional data reveals metabolic modules that regulate macrophage polarization. Immunity 2015; 42:419-30; PMID:25786174; http://dx.doi.org/10.1016/j.immuni.2015.02.005
39. Everts B, Amiel E, Huang SC-C, Smith AM, Chang C-H, Lam WY, Redmann V, Freitas TC, Blagih J, van der Windt GJW et al. TLR-driven early glycolytic reprogramming via the kinases TBK1-IKK alpha supports the anabolic demands of dendritic cell activation. Nat Immunol 2014; 15:323-32; PMID:24562310; http://dx.doi.org/10.1038/ni.2833
40. Biswas Subhra K. Metabolic reprogramming of immune cells in cancer progression. Immunity 2015; 43:435-49; PMID:26377897; http://dx.doi.org/10.1016/j.immuni.2015.09.001
41. Son J, Lyssiotis CA, Ying H, Wang X, Hua S, Ligorio M, Perera RM, Ferrone CR, Mullarky E, Shyh-Chang N et al. Glutamine supports pancreatic cancer growth through a KRAS-regulated metabolic pathway. Nature 2013; 496:101-5; PMID:23535601; http://dx.doi.org/10.1038/nature12040

42. O'Neill LAJ, Hardie DG. Metabolism of inflammation limited by AMPK and pseudo-starvation. Nature 2013; 493:346-55; PMID:23325217; http://dx.doi.org/10.1038/nature11862
43. Heid ME, Keyel PA, Kamga C, Shiva S, Watkins SC, Salter RD. Mitochondrial reactive oxygen species induces NLRP3-dependent lysosomal damage and inflammasome activation. J Immunol 2013; 191:5230-8; PMID:24089192; http://dx.doi.org/10.4049/jimmunol.1301490
44. Incio J, Suboj P, Chin SM, Vardam-Kaur T, Liu H, Hato T, Babykutty S, Chen I, Deshpande V, Jain RK et al. Metformin reduces desmoplasia in pancreatic cancer by reprogramming stellate cells and tumor-associated macrophages. PLoS One 2015; 10:e0141392; PMID:26641266; http://dx.doi.org/10.1371/journal.pone.0141392
45. Chang C-H, Qiu J, O'sullivan D, Buck Michael D, Noguchi T, Curtis Jonathan D, Chen Q, Gindin M, Gubin Matthew M, van der Windt Gerritje JW et al. Metabolic competition in the tumor microenvironment is a driver of cancer progression. Cell 2015; 162:1229-41; PMID:26321679; http://dx.doi.org/10.1016/j.cell.2015.08.016
46. Vander Heiden MG. Targeting cancer metabolism: a therapeutic window opens. Nat Rev Drug Discov 2011; 10:671-84; PMID:21878982; http://dx.doi.org/10.1038/nrd3504
47. Shin Y, Han S, Jeon JS, Yamamoto K, Zervantonakis IK, Sudo R, Kamm RD, Chung S. Microfluidic assay for simultaneous culture of multiple cell types on surfaces or within hydrogels. Nat Protocols 2012; 7:1247-59; PMID:22678430; http://dx.doi.org/10.1038/nprot.2012.051
48. Selvarasu S, Ho YS, Chong WPK, Wong NSC, Yusufi FNK, Lee YY, Yap MGS, Lee D-Y. Combined in silico modeling and metabolomics analysis to characterize fed-batch CHO cell culture. Biotechnology and Bioengineering 2012; 109:1415-29; PMID:22252269; http://dx.doi.org/10.1002/bit.24445
49. Smith CA, Want EJ, O'Maille G, Abagyan R, Siuzdak G. XCMS: processing mass spectrometry data for metabolite profiling using nonlinear peak alignment, matching, and identification. Anal Chem 2006; 78:779-87; PMID:16448051; http://dx.doi.org/10.1021/ac051437y
50. Blum R, Kloog Y. Metabolism addiction in pancreatic cancer. Cell Death Dis 2014; 5:e1065; PMID:24556680; http://dx.doi.org/10.1038/cddis.2014.38